

The Channel Between Randomly Oriented Dipoles: Statistics and Outage in the Near and Far Field

Gregor Dumphart and Armin Wittneben
Wireless Communications Group, D-ITET, ETH Zurich
Zürich, Switzerland
Email: {dumphart, wittneben}@nari.ee.ethz.ch

Abstract—We consider the class of wireless links whose propagation characteristics are described by a dipole model. This comprises free-space links between dipole antennas and magneto-inductive links between coils, with important communication and power transfer applications. A dipole model describes the channel coefficient as a function of link distance and antenna orientations. In many use cases the orientations are random, causing a random fading channel. This paper presents a closed-form description of the channel statistics and the resulting outage performance for the case of i.i.d. uniformly distributed antenna orientations in 3D space. For reception in AWGN after active transmission, we show that the high-SNR outage probability scales like $p_e \propto \text{SNR}^{-1/2}$ in the near- or far-field region, i.e. the diversity exponent is just 1/2 (even 1/4 with backscatter or load modulation). The diversity exponent improves to 1 in the near-far-field transition due to polarization diversity. Analogous statements are made for the power transfer efficiency and outage capacity.

Index Terms—fading, outage, polarization diversity, dipole antennas, loop antennas, coil misalignment, backscatter

I. INTRODUCTION

Wireless engineers often rely on statistical channel models to describe complicated propagation environments and their fading characteristics. Fading occurs when (for a narrowband channel) the random channel coefficient $h \in \mathbb{C}$ is close to zero, i.e. $h \approx 0$, which can cause a link outage [1]. A statistical channel model allows to study the performance implications of fading analytically. For example, for a digital modulation scheme with transmit power P , Rayleigh fading $h \sim \mathcal{CN}(0, \sigma^2)$ due to rich multipath propagation, and additive white Gaussian noise (AWGN), the bit error rate is asymptotically proportional to P^{-L} with $L = 1$. The small diversity exponent L means that Rayleigh fading hinders reliable low-power communication [1, Cpt. 3]. The existing literature states many such performance results for various models, e.g. see [2].

Fading events $h \approx 0$ can be caused by mechanisms other than multipath propagation or shadowing; they can even occur in free space in the case of inopportune antenna orientations. For example, the transmitter-to-receiver (TX-to-RX) direction may coincide with a zero of the TX-antenna radiation pattern or the RX antenna may be misaligned with the incident field [3]. To that effect, non-isotropic antennas with random orientations can give rise to a fading channel with random channel coefficient h , even in free space [4], [5]. Such random antenna orientations are to be expected for wireless applications with high mobility or application-specific

node locations. Associated fading channels have been studied in [4] for mobile radio devices and in [6], [7] for magnetic induction links between randomly arranged coils.

In this paper we study fading due to random antenna orientations for the class of wireless links that can be adequately modeled by a free-space link from a TX dipole to a RX dipole. This comprises:

- Magnetic induction links between two weakly coupled coils (loop antennas).
- Capacitive links between small electric dipole antennas.
- Links between $\lambda/2$ -length dipole antennas in free space.
- Links from a magnetic dipole to a small loop or from an electric dipole to a pair of terminals with small separation.

Those have important applications in wireless power transfer and data communication, either with an active TX or a passive tag (RFID load modulation or backscatter modulation). [8]

The statistics and communication-theoretic performance aspects of this fading channel are, to the best of our knowledge, not covered by existing work. The need for an appropriate statistical channel model was highlighted in [9] where, because of the lack of a better model, a Rayleigh fading model was assumed for RFID links. Similarly, the heuristic assumption of a Gaussian-distributed data rate was made in [10] for a randomly arranged magnetic induction link.

Contribution: This paper contains the following novel results for links between dipoles with uniformly distributed 3D orientations, presented in communication-theoretic parlance.

- We derive the channel statistics for the near- and far-field region. We show that the outage behavior is characterized by a diversity exponent of just $\frac{1}{2}$.
- We derive the channel statistics in the near-far-field transition and demonstrate a diversity exponent of 1.
- An outage analysis demonstrates the severity of this fading channel in terms of the behavior of the outage PTE, outage capacity, and bit error probability.

Related Work: Regarding misaligned magnetic-induction links, most studies focused on small lateral or angular deviations in the regime of short-range power transfer [11], [12] where the specific coil geometries must be considered. The concept of outage probability, diversity exponent and outage capacity in relation to fading is well-established for multipath radio channels [1]. Likewise, polarization diversity is a well-established concept [13, Sec. 2.5]. The work in [10] identified

the outage capacity as a meaningful performance measure of randomly arranged magneto-inductive communication links. The distribution in (13) and various results on diversity combining appeared in our paper [6]. The contents of this paper are also contained in the dissertation of the first author [14].

Paper Structure: Sec. II describes the dipole model in detail. The rather technical Sec. III then derives the channel statistics between randomly oriented antennas, which enables the subsequent outage and diversity analysis in Sec. IV. After commenting on the implications for RFID and backscatter systems in Sec. V, we conclude the paper in Sec. VI.

II. DIPOLE CHANNEL MODEL

We consider a narrowband wireless link from a transmitting dipole, driven by a TX amplifier, to a receiving dipole which feeds a low-noise amplifier or tank circuit. The link geometry is shown in Fig. 1 and is described by the link distance r and three unit vectors: the TX and RX dipole axis directions $\mathbf{o}_T, \mathbf{o}_R \in \mathbb{R}^3$ and the TX-to-RX direction $\mathbf{u} \in \mathbb{R}^3$.

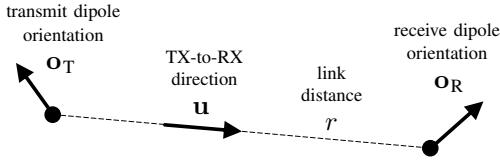


Fig. 1. Geometry of a link between dipoles with arbitrary orientations $\mathbf{o}_T, \mathbf{o}_R \in \mathbb{R}^3$ (unit vectors) and distance r . The model serves as a description of unaligned links between weakly coupled coils or between dipole antennas.

The channel coefficient $h \in \mathbb{C}$ is given by [3], [14]

$$h = \alpha \left(\left(\frac{1}{(kr)^3} + \frac{j}{(kr)^2} \right) J_{\text{NF}} + \frac{1}{2kr} J_{\text{FF}} \right) \quad (1)$$

where $k = \frac{2\pi}{\lambda} = \frac{2\pi f}{c}$ is the wavenumber and j the imaginary unit. The prefactor α is of no formal importance for this paper. It is given by $\alpha = \bar{\alpha} e^{-jkr}$ where $\bar{\alpha} \in \mathbb{C}$ subsumes technical parameters (e.g., coil diameters) which are described in the appendix together with the detailed model conditions.

The RX may be located in the near-field region ($kr \ll 1$) or the far-field region ($kr \gg 1$), or in the transition in between. The formula (1) uses the near- and far-field alignment factors, given by the inner products

$$J_{\text{NF}} = \mathbf{o}_R^T \boldsymbol{\beta}_{\text{NF}}, \quad J_{\text{NF}} \in [-1, 1], \quad (2)$$

$$J_{\text{FF}} = \mathbf{o}_R^T \boldsymbol{\beta}_{\text{FF}}, \quad J_{\text{FF}} \in [-1, 1]. \quad (3)$$

They account for signal attenuation due to suboptimal node orientations (misalignment). The formulas use unitless field vector quantities $\boldsymbol{\beta}_{\text{NF}}$ and $\boldsymbol{\beta}_{\text{FF}}$, which we call the scaled near field and the scaled far field, respectively. They are given by

$$\boldsymbol{\beta}_{\text{NF}} = \frac{1}{2}(3\mathbf{u}\mathbf{u}^T - \mathbf{I}_3) \mathbf{o}_T, \quad (4)$$

$$\boldsymbol{\beta}_{\text{FF}} = (\mathbf{I}_3 - \mathbf{u}\mathbf{u}^T) \mathbf{o}_T \quad (5)$$

and illustrated in Fig. 2. The formulas use a convenient linear-algebraic formalism, which has been derived in our previous

work [14, App. A] from an existing trigonometric description of the dipole field [3]. The field magnitudes are given by

$$\beta_{\text{NF}} = \|\boldsymbol{\beta}_{\text{NF}}\| = \frac{1}{2} \sqrt{1 + 3(\mathbf{u}^T \mathbf{o}_T)^2}, \quad \frac{1}{2} \leq \beta_{\text{NF}} \leq 1, \quad (6)$$

$$\beta_{\text{FF}} = \|\boldsymbol{\beta}_{\text{FF}}\| = \sqrt{1 - (\mathbf{u}^T \mathbf{o}_T)^2}, \quad 0 \leq \beta_{\text{FF}} \leq 1. \quad (7)$$

The far-field magnitude β_{FF} can fade to zero but β_{NF} can not, as can be seen in Fig. 2.

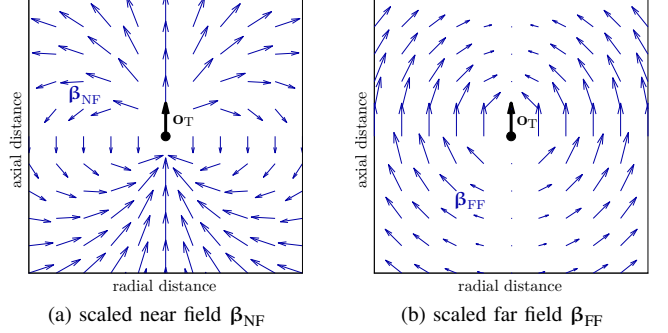


Fig. 2. Scaled near and far field around a transmitting dipole with vertical axis orientation (unit vector \mathbf{o}_T). By definition these fields do not comprise path loss; the maximum magnitude is 1. In particular, $\beta_{\text{NF}} = 1, \beta_{\text{FF}} = 0$ hold on the dipole axis while $\beta_{\text{NF}} = \frac{1}{2}, \beta_{\text{FF}} = 1$ hold in the perpendicular plane.

We shall point out two specific dipole arrangements:

- Dipoles in coaxial arrangement $\mathbf{o}_T = \mathbf{o}_R = \mathbf{u}$:
in this case $J_{\text{NF}} = 1, J_{\text{FF}} = 0$, and thus $h = h_{\text{coax}}$ with

$$h_{\text{coax}} = \alpha \left(\frac{1}{(kr)^3} + \frac{j}{(kr)^2} \right). \quad (8)$$

- Dipoles in parallel arrangement $\mathbf{o}_T = \mathbf{o}_R$ with $\mathbf{u}^T \mathbf{o}_T = 0$:
in this case $J_{\text{NF}} = -\frac{1}{2}, J_{\text{FF}} = 1$ and thus $h = h_{\text{para}}$ with

$$h_{\text{para}} = \frac{\alpha}{2} \left(-\frac{1}{(kr)^3} - \frac{j}{(kr)^2} + \frac{1}{kr} \right). \quad (9)$$

We note that $\eta = |h|^2$ is the power transfer efficiency (PTE) over the link. An important quantity is the maximum PTE given kr and α , denoted as $\eta_{\text{opt}} = |h_{\text{opt}}|^2$. We find that¹

$$\eta_{\text{opt}} = |h_{\text{opt}}|^2 = \max_{\mathbf{o}_T, \mathbf{o}_R} |h|^2 = \begin{cases} |h_{\text{coax}}|^2 & \text{if } kr \leq kr_{\text{th}} \\ |h_{\text{para}}|^2 & \text{if } kr > kr_{\text{th}} \end{cases} \quad (10)$$

whereby the threshold fulfills $|h_{\text{coax}}| = |h_{\text{para}}|$. It is given by

$$kr_{\text{th}} = \sqrt{\frac{\sqrt{37} + 5}{2}} \approx 2.3540. \quad (11)$$

¹To prove the statement (10), we write h as bilinear form $h = \mathbf{o}_R^T \mathbf{A} \mathbf{o}_T$ and deduce $\mathbf{A} = \alpha \left(\left(\frac{1}{(kr)^3} + \frac{j}{(kr)^2} \right) \left(\frac{3}{2} \mathbf{u}\mathbf{u}^T - \frac{1}{2} \mathbf{I}_3 \right) + \frac{1}{2kr} (\mathbf{I}_3 - \mathbf{u}\mathbf{u}^T) \right) \in \mathbb{C}^{3 \times 3}$ from (1) to (5). We find that h_{coax} is an eigenvalue by verifying $\mathbf{A}\mathbf{u} = h_{\text{coax}}\mathbf{u}$. Furthermore, h_{para} is a double eigenvalue because $\mathbf{A}\mathbf{u}_\perp = h_{\text{para}}\mathbf{u}_\perp$ for any vector \mathbf{u}_\perp that is orthogonal to \mathbf{u} . Therefore, the statement (10) follows from basic linear algebra. The threshold kr_{th} in (11) is found by solving the equation $|h_{\text{coax}}|^2 = |h_{\text{para}}|^2$ for kr , using the definitions (8) and (9).

III. CHANNEL STATISTICS

Our starting point is the assumption that the TX and RX antenna orientations (unit vectors) are random and statistically independent, with uniform distributions

$$\mathbf{o}_T, \mathbf{o}_R \stackrel{\text{i.i.d.}}{\sim} \mathcal{U}(\mathcal{S}) \quad (12)$$

on the unit sphere $\mathcal{S} \subset \mathbb{R}^3$. The quantities α, k, r, \mathbf{u} are considered non-random throughout. Hence, the statistics of h in (1) are determined by the joint statistics of $J_{\text{NF}}, J_{\text{FF}}$.

A. In the Near-Field Region or Far-Field Region

First, we address the important marginal distributions of J_{NF} and J_{FF} which describe the statistics of h in the near-field region ($kr \ll kr_{\text{th}}$) and the far-field region ($kr \gg kr_{\text{th}}$), respectively.

Proposition 1. Assume (12). Then the near-field alignment factor J_{NF} has the marginal probability density function (PDF)

$$f_{J_{\text{NF}}}(J_{\text{NF}}) = \frac{1}{2\beta_{\text{NF}}} \cdot \begin{cases} 1 & |J_{\text{NF}}| \leq \frac{1}{2} \\ 1 - \frac{\text{arcosh}(2|J_{\text{NF}}|)}{\text{arcosh}(2)} & \frac{1}{2} < |J_{\text{NF}}| < 1 \\ 0 & 1 \leq |J_{\text{NF}}| \end{cases} \quad (13)$$

with $\beta_{\text{NF}} = \frac{\sqrt{3}}{2 \text{arcosh}(2)}$. The far-field alignment factor exhibits

$$f_{J_{\text{FF}}}(J_{\text{FF}}) = \frac{1}{2} \left(\frac{\pi}{2} - \arcsin |J_{\text{FF}}| \right) \cdot \mathbb{1}_{[-1,1]}(J_{\text{FF}}). \quad (14)$$

Thereby, $\mathbb{1}_{[-1,1]}$ is the indicator function for this interval. The PDFs are shown in Fig. 3a and 3b.

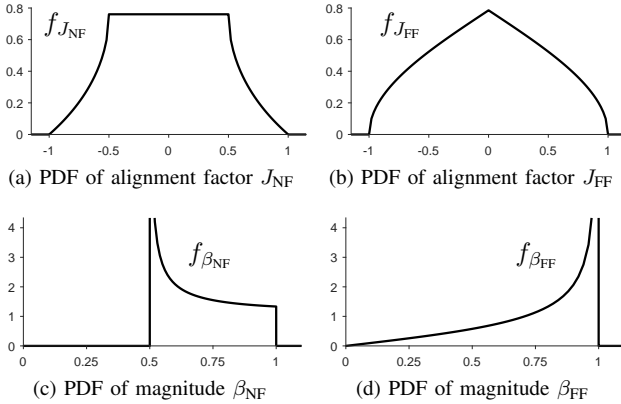


Fig. 3. Marginal PDFs arising from random antenna orientations on both ends with uniform distributions in 3D.

Proof. We will heavily use the fact that, for a random constant-length vector in \mathbb{R}^3 with uniform distribution on a sphere, any projection has uniform distribution. This fact is a corollary of Archimedes' hat-box theorem or of the fact that the lateral surface area of a sphere cap is linear in its height (which implies a linear CDF for a projection, cf. [6]). A first implication to our formalism is that the TX-side projection $\mathbf{u}^T \mathbf{o}_T$, which determines the magnitudes β_{NF} and β_{FF} , has uniform distribution $\mathbf{u}^T \mathbf{o}_T \sim \mathcal{U}(-1, 1)$ due to $\mathbf{o}_T \sim \mathcal{U}(\mathcal{S})$.

Consequently, with a basic change-of-variables calculation we obtain from (6) and (7) the PDFs of the field magnitudes

$$f_{\beta_{\text{NF}}}(\beta_{\text{NF}}) = \frac{4}{\sqrt{3}} \frac{\beta_{\text{NF}}}{\sqrt{4\beta_{\text{NF}}^2 - 1}} \cdot \mathbb{1}_{[\frac{1}{2}, 1]}(\beta_{\text{NF}}), \quad (15)$$

$$f_{\beta_{\text{FF}}}(\beta_{\text{FF}}) = \frac{\beta_{\text{FF}}}{\sqrt{1 - \beta_{\text{FF}}^2}} \cdot \mathbb{1}_{[0, 1]}(\beta_{\text{FF}}) \quad (16)$$

which are shown in Fig. 3c and 3d. The random RX orientation $\mathbf{o}_R \sim \mathcal{U}(\mathcal{S})$ in (2) and (3) results in conditional distributions $J_{\text{NF}} | \beta_{\text{NF}} \sim \mathcal{U}(-\beta_{\text{NF}}, \beta_{\text{NF}})$ and $J_{\text{FF}} | \beta_{\text{FF}} \sim \mathcal{U}(-\beta_{\text{FF}}, \beta_{\text{FF}})$. The joint PDFs $f_{J_{\text{NF}} | \beta_{\text{NF}}} \cdot f_{\beta_{\text{NF}}}$ and $f_{J_{\text{FF}} | \beta_{\text{FF}}} \cdot f_{\beta_{\text{FF}}}$ yield $f_{J_{\text{NF}}}$ and $f_{J_{\text{FF}}}$ via marginalization integrals (the steps are omitted). \square

Proposition 2. Consider the cumulative distribution function (CDF) $F_{|h|^2}(s) = \mathbb{P}[|h|^2 \leq s]$. In the near-field region $kr \ll kr_{\text{th}}$ (described by $J_* = J_{\text{NF}}$) or the far-field region $kr \gg kr_{\text{th}}$ (described by $J_* = J_{\text{FF}}$), the approximation

$$F_{|h|^2}(s) \approx \frac{2 \cdot f_{J_*}(0)}{|h_{\text{opt}}|} \sqrt{s} \quad (17)$$

applies under assumption (12). It is accurate for $s \ll |h_{\text{opt}}|^2$.

Proof. Either case fulfills $|h|^2 \approx |h_{\text{opt}}|^2 J_*^2$. We calculate

$$\begin{aligned} F_{|h|^2}(s) &\approx F_{J_*^2} \left(\frac{s}{|h_{\text{opt}}|^2} \right) = \mathbb{P} \left[|J_*| \leq \frac{\sqrt{s}}{|h_{\text{opt}}|} \right] \\ &= 2 \int_0^{\frac{\sqrt{s}}{|h_{\text{opt}}|}} f_{J_*}(x) dx \leq 2 \cdot f_{J_*}(0) \int_0^{\frac{\sqrt{s}}{|h_{\text{opt}}|}} dx. \end{aligned} \quad (18)$$

This bound is tight for small integration intervals because the integrand is continuous, as seen in Fig. 3a and 3b. \square

The CDF behavior $F_{|h|^2}(s) \propto \sqrt{s}$ for small s hints that fading events $|h|^2 \approx 0$ occur with significant probability. This is due to the probability densities $f_{J_{\text{NF}}}(0) > 0$, $f_{J_{\text{FF}}}(0) > 0$.

B. Near-Far Transition with Random Receiver Orientation

We consider the statistics of $h \in \mathbb{C}$ when both near- and far-field propagation make significant contributions. First, we consider the case of a random RX orientation $\mathbf{o}_R \sim \mathcal{U}(\mathcal{S})$ while \mathbf{o}_T and \mathbf{u} are fixed. This interesting case will serve as preparation for the fully random case.

We start our mathematical approach by observing from (1) to (3) that the channel coefficient is an inner product

$$h = \mathbf{o}_R^T \mathbf{v}, \quad \mathbf{o}_R \in \mathbb{R}^3, \quad \mathbf{v} \in \mathbb{C}^3 \quad (19)$$

of the random \mathbf{o}_R and a unitless, complex-valued field vector

$$\mathbf{v} = \alpha \left(\left(\frac{1}{(kr)^3} + \frac{j}{(kr)^2} \right) \boldsymbol{\beta}_{\text{NF}} + \frac{1}{2kr} \boldsymbol{\beta}_{\text{FF}} \right). \quad (20)$$

This field vector is non-random in this context because it is determined by the non-random $\alpha, kr, \mathbf{u}, \mathbf{o}_T$. We consider $\mathbf{v}_{\text{Re}} = \text{Re}(\mathbf{v})$ and $\mathbf{v}_{\text{Im}} = \text{Im}(\mathbf{v})$ and note that these two vectors are linearly independent unless $\mathbf{u}^T \mathbf{o}_T = 0$ or $\mathbf{u}^T \mathbf{o}_T = \pm 1$; the simple proof thereof is omitted.

The random channel coefficient is expressed as

$$h = \text{Re}(h) + j \cdot \text{Im}(h) = \mathbf{o}_R^T \mathbf{v}_{\text{Re}} + j \cdot \mathbf{o}_R^T \mathbf{v}_{\text{Im}}, \quad (21)$$

which exhibits a statistical dependence between the real and imaginary part because the random \mathbf{o}_R affects both. In the following, we specify the statistics of h in terms of the conditional PDF $f(h|\mathbf{o}_T) = f(h|\mathbf{v})$.

Proposition 3. Consider a random unit vector $\mathbf{o}_R \sim \mathcal{U}(S)$, i.e. with uniform distribution on the unit sphere in \mathbb{R}^3 , and a non-random vector $\mathbf{v} = \mathbf{v}_{Re} + j \cdot \mathbf{v}_{Im} \in \mathbb{C}^3$ with linearly independent $\mathbf{v}_{Re}, \mathbf{v}_{Im} \in \mathbb{R}^3$. Let $v_{Re} = \|\mathbf{v}_{Re}\|$, $v_{Im} = \|\mathbf{v}_{Im}\|$, and $\rho = \frac{\mathbf{v}_{Re}^T \mathbf{v}_{Im}}{v_{Re} v_{Im}}$ (correlation coefficient). Then the joint PDF of the projections $\text{Re}(h) = \mathbf{o}_R^T \mathbf{v}_{Re}$ and $\text{Im}(h) = \mathbf{o}_R^T \mathbf{v}_{Im}$ is

$$f(h|\mathbf{v}) = f(\text{Re}(h), \text{Im}(h) | \mathbf{v}_{Re}, \mathbf{v}_{Im}) = \frac{1}{v_{Re} v_{Im} \sqrt{1-\rho^2}} \psi \left(\left\| \begin{bmatrix} 1 & 0 \\ \rho & \sqrt{1-\rho^2} \end{bmatrix}^{-1} \begin{bmatrix} \text{Re}(h)/v_{Re} \\ \text{Im}(h)/v_{Im} \end{bmatrix} \right\|^2 \right) \quad (22)$$

with $\psi(x) = \frac{1}{2\pi\sqrt{1-x}} \mathbb{1}_{[0,1]}(x)$. The uniform marginal distributions $h_{Re} \sim \mathcal{U}(-v_{Re}, v_{Re})$ and $h_{Im} \sim \mathcal{U}(-v_{Im}, v_{Im})$ apply.

Proof. We apply the Gram-Schmidt process to $\mathbf{v}_{Re}, \mathbf{v}_{Im}$ to obtain orthonormal vectors $\mathbf{m} = \frac{\mathbf{v}_{Re}}{v_{Re}}$, $\mathbf{n} = \frac{(\mathbf{I}_3 - \mathbf{m}\mathbf{m}^T)\mathbf{v}_{Im}}{\|(\mathbf{I}_3 - \mathbf{m}\mathbf{m}^T)\mathbf{v}_{Im}\|}$. They fulfill $\mathbf{v}_{Re} = v_{Re}\mathbf{m}$ and $\mathbf{v}_{Im} = v_{Im}\rho\mathbf{m} + v_{Im}\sqrt{1-\rho^2}\mathbf{n}$. Written as linear map, $\begin{bmatrix} \mathbf{v}_{Re} & \mathbf{v}_{Im} \end{bmatrix} = \begin{bmatrix} \mathbf{m} & \mathbf{n} \end{bmatrix} \mathbf{E}^T$. The projections of \mathbf{o}_R thus fulfill $\begin{bmatrix} \text{Re}(h) & \text{Im}(h) \end{bmatrix} = \mathbf{o}_R^T \begin{bmatrix} \mathbf{m} & \mathbf{n} \end{bmatrix} \mathbf{E}^T = \begin{bmatrix} m_o & n_o \end{bmatrix} \mathbf{E}^T$. The joint PDF f_{m_o, n_o} is given by Lemma 1 below. We subsequently obtain the PDF of $\text{Re}(h), \text{Im}(h)$ with a change-of-variables argument: for random m_o, n_o with PDF f_{m_o, n_o} and an invertible linear map \mathbf{E} , the PDF $f(\text{Re}(h), \text{Im}(h) | \mathbf{v}) = \frac{1}{\det(\mathbf{E})} f_{m_o, n_o}(\mathbf{E}^{-1}[\text{Re}(h) \ \text{Im}(h)]^T)$ applies. \square

Lemma 1. Consider orthonormal vectors $\mathbf{m}, \mathbf{n} \in \mathbb{R}^3$ and a random unit vector $\mathbf{o} \sim \mathcal{U}(S)$. The joint PDF of $m_o = \mathbf{o}^T \mathbf{m}$, $n_o = \mathbf{o}^T \mathbf{n}$ is then given by $f_{m_o, n_o}(m_o, n_o) = \psi(m_o^2 + n_o^2)$.

For the proof of Lemma 1 we refer to [14, Lemma 4.5]. We note that the distribution $h|\mathbf{o}_T$ is equivalent to $h|\mathbf{u}^T \mathbf{o}_T$ because $\mathbf{o}_R \sim \mathcal{U}(S)$ has rotational invariance. Thus,

$$f(h|\mathbf{o}_T) = f(h|\mathbf{v}) = f(h|\mathbf{u}^T \mathbf{o}_T). \quad (23)$$

An evaluation of this conditional PDF is shown in Fig. 4 for the exemplary value $\mathbf{u}^T \mathbf{o}_T = 0.3$.

Proposition 4. Let h be distributed according to Prop. 3. Then the CDF $F_{|h|^2}$ is within the bounds

$$\frac{s}{2b} \leq F_{|h|^2|\mathbf{v}}(s|\mathbf{v}) \leq \frac{s}{2b} \left(1 - \frac{s}{s_0}\right)^{-1/2} \quad (24)$$

if $s < s_0$, whereby $s_0 = a - \sqrt{a^2 - b^2}$ with $a = \frac{1}{2}(v_{Re}^2 + v_{Im}^2)$ and $b = v_{Re} v_{Im} \sqrt{1-\rho^2}$.

Proof. The joint PDF of $\begin{bmatrix} \text{Re}(h) & \text{Im}(h) \end{bmatrix} = \mathbf{o}_R^T \begin{bmatrix} \mathbf{v}_{Re} & \mathbf{v}_{Im} \end{bmatrix}$ is given by Prop. 3. There, a linear map $\mathbf{E} \in \mathbb{R}^{2 \times 2}$ maps from the closed unit disk to the ellipse that is the support of $f(h|\mathbf{v})$. Let s_0 be the smaller eigenvalue of $\mathbf{E}^T \mathbf{E}$; the stated formula is obtained from the characteristic polynomial. Now $s < s_0$ guarantees that $f(h|\mathbf{v}) < \infty$ because then h

is in the interior of $\text{supp} f(h|\mathbf{v})$. In particular, $f(h|\mathbf{v}) = \frac{\psi(\|\mathbf{E}^{-1}[\text{Re}(h) \ \text{Im}(h)]^T\|^2)}{b} \leq \frac{\psi(s/s_0)}{b}$. We find the upper bound via $P[|h|^2 \leq s|\mathbf{v}] = \int_{|h|^2 \leq s} f(h|\mathbf{v}) dh \leq \frac{\psi(s/s_0)}{b} \int_{|h|^2 \leq s} dh = \frac{\psi(s/s_0) \cdot \pi s}{b} = \frac{s}{2b} / \sqrt{1-s/s_0}$. Analogously, the lower bound is due to $f(h|\mathbf{v}) \geq \frac{\psi(0)}{b} = \frac{1}{2\pi b}$ for $s < s_0$. \square

In essence, Prop. 4 states that $F_{|h|^2}(s) \propto s$ for small s in the transition region. In contrary, the near- and far-field region behavior $F_{|h|^2}(s) \propto \sqrt{s}$ from Prop. 2 exhibits a larger concentration of probability mass near $|h|^2 = 0$. The advantage of the transition region is caused by the sum of phase-shifted field vectors in (20) providing polarization diversity: a deep fade $h = 0$ can only occur if \mathbf{o}_R is orthogonal to both \mathbf{v}_{Re} and \mathbf{v}_{Im} . In other words, the field vector $\text{Re}(\mathbf{v}e^{j2\pi ft})$ now oscillates on an ellipse, not on a line [13, Sec. 2.5].

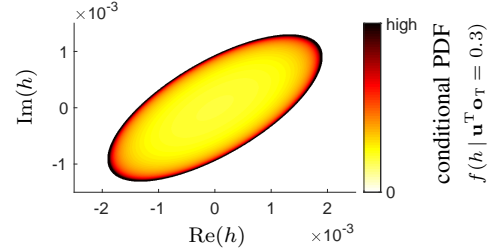


Fig. 4. Conditional PDF of the channel coefficient $h \in \mathbb{C}$ for random RX orientation \mathbf{o}_R , described by Prop. 3 in closed form. This evaluation assumes the values $\mathbf{u}^T \mathbf{o}_T = 0.3$, $kr = 2$, $\bar{\alpha} = 10^{-2}$.

C. Near-Far Transition, Random Orientations at Both Ends

Finally, we address the distribution of h in the fully-random case $\mathbf{o}_T, \mathbf{o}_R \stackrel{\text{i.i.d.}}{\sim} \mathcal{U}(S)$, again under consideration of all terms in (1). Fig. 5 shows scatter plots of h for various kr values.

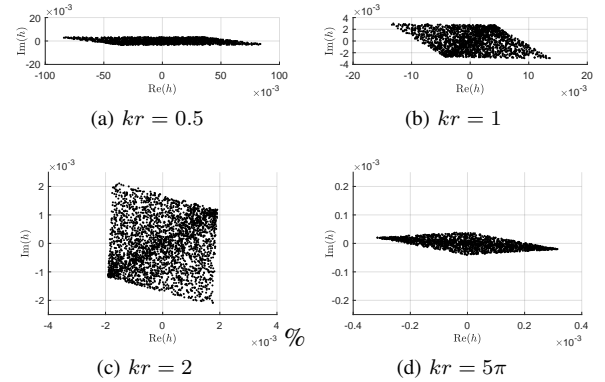


Fig. 5. Scatter plots of the random channel coefficient $h \in \mathbb{C}$ between two dipoles with random orientations $\mathbf{o}_T, \mathbf{o}_R \sim \mathcal{U}(S)$ for different regions. For $kr \ll kr_{th}$ or $kr \gg kr_{th}$, all samples lie on a line. The plots were obtained with random sampling and $\bar{\alpha} = 10^{-2}$ was assumed.

Proposition 5. Under (12) and based on the conditional PDF $f(h|\mathbf{u}^T \mathbf{o}_T) = f(h|\mathbf{v})$ from Prop. 3, the PDF of h is given by

$$f(h) = \frac{1}{2} \cdot \int_{-1}^{+1} f(h|\mathbf{u}^T \mathbf{o}_T = x) dx. \quad (25)$$

Proof. We find $f(h) = \int_{-1}^{+1} f(h|\mathbf{u}^T \mathbf{o}_T = x) f(\mathbf{u}^T \mathbf{o}_T = x) dx$ from (23) and marginalization. With $\mathbf{o}_T \sim \mathcal{U}(\mathcal{S})$ while \mathbf{u} is non-random, the uniform distribution $\mathbf{u}^T \mathbf{o}_T \sim \mathcal{U}(-1, 1)$ applies (see the proof of Prop. 1). Thus $f(\mathbf{u}^T \mathbf{o}_T) = \frac{1}{2}$. \square

A closed-form solution of the integral (25) is unavailable, but an evaluation obtained with numerical integration is shown in Fig. 6a. The results are supplemented by the geometric explanation of the rhombus-shaped support of the distribution in Fig. 6b.

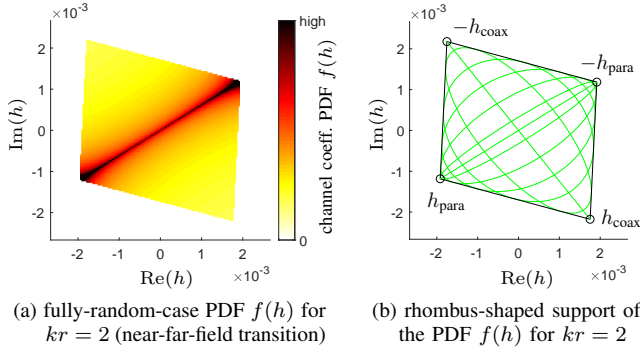


Fig. 6. PDF of the random channel coefficient $h \in \mathbb{C}$ for random dipole orientations $\mathbf{o}_T, \mathbf{o}_R \sim \mathcal{U}(\mathcal{S})$, evaluated here for $kr = 2$ and $\bar{\alpha} = 10^{-2}$. The PDF was computed by solving (25) numerically. Fig. 6b shows how the rhombus-shaped support $\text{supp } f(h)$ arises from a union of ellipses $\text{supp } f(h|\mathbf{u}^T \mathbf{o}_T)$, shown for $\mathbf{u}^T \mathbf{o}_T \in \{0, .1, .3, .5, .7, .9, 1\}$. For $\mathbf{u}^T \mathbf{o}_T \in \{0, 1\}$ the ellipse becomes a line. The ellipses for $\mathbf{u}^T \mathbf{o}_T \approx 0$ cause a concentration of probability mass between $\pm h_{\text{para}}$.

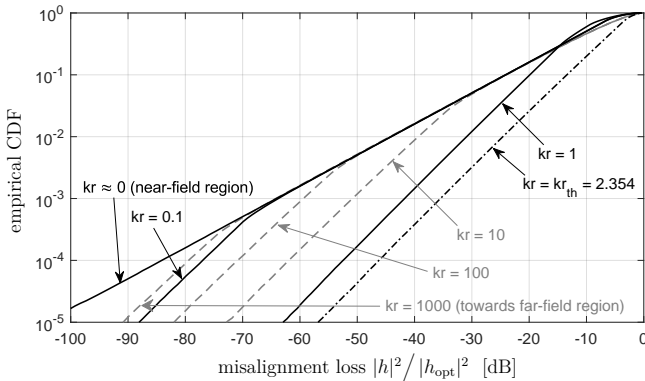


Fig. 7. Statistics of the channel attenuation due to random TX and RX orientations, computed via Monte Carlo simulation for i.i.d. uniform distributions in 3D. We observe that severe misalignment loss occurs with significant probability, especially in the near-field region and the far-field region. The near-far-field transition features a beneficial polarization diversity effect.

We argue that, via (25), the beneficial property $F_{|h|^2}(s) \propto s$ for small s carries over from $F_{|h|^2|\mathbf{v}}(s|\mathbf{v}) \propto s$ in Prop. 4. This is supported by the Monte-Carlo simulation in Fig. 7, but a rigorous argument is unavailable. A non-rigorous argument is that polarization diversity (i.e. linearly independent $\mathbf{v}_{\text{Re}}, \mathbf{v}_{\text{Im}}$) occurs with probability 1. Put differently, a problematic case $\mathbf{u}^T \mathbf{o}_T = 0$ or $\mathbf{u}^T \mathbf{o}_T = \pm 1$, where the boundary ellipse of $\text{supp } f_{h|\mathbf{u}^T \mathbf{o}_T}$ degenerates to a line, occurs with probability 0.

IV. OUTAGE ANALYSIS

A. Outage Power Transfer Efficiency η_ϵ

The power transfer efficiency (PTE) $\eta = |h|^2$ is a random variable in the context of this paper. Analogous to the concept of outage capacity [1], we consider the outage PTE, defined as the PTE value η_ϵ for which an outage event $|h|^2 < \eta_\epsilon$ occurs with a certain probability ϵ . The CDF of $|h|^2$ describes this very dependence: $\epsilon = F_{|h|^2}(\eta_\epsilon)$.

Proposition 6. Assume (12) and that the RX is in the near-field region ($J_* = J_{\text{NF}}$) or the far-field region ($J_* = J_{\text{FF}}$). Then, a target PTE η_ϵ results in an outage probability

$$\epsilon = F_{|h|^2}(\eta_\epsilon) \approx 2 \cdot f_{J_*}(0) \sqrt{\frac{\eta_\epsilon}{\eta_{\text{opt}}}}. \quad (26)$$

Vice versa, a target outage probability ϵ yields the outage PTE

$$\eta_\epsilon = F_{|h|^2}^{-1}(\epsilon) \approx \frac{\epsilon^2 \eta_{\text{opt}}}{(2 \cdot f_{J_*}(0))^2}. \quad (27)$$

The approximations are accurate for $\eta_\epsilon \ll \eta_{\text{opt}}$.

Proof. The statements follow directly from Prop. 2. \square

From (26) and (27) we observe the proportionality $\epsilon \propto \eta_{\text{opt}}^{-\frac{1}{2}}$ as well as $\eta_\epsilon \propto \epsilon^2$. This scaling behavior demonstrates the drastic fading effect due to random antenna orientations. On the one hand, increasing η_{opt} (e.g., by improving technical parameters or reducing the distance) is not an efficient means for reducing ϵ . On the other hand, requiring some degree of reliability (i.e. a small ϵ) is associated with an extremely small PTE η_ϵ . For example, aiming for a factor-10 improvement of ϵ demands a 20 dB loss for η_ϵ .

The situation improves in the near-far-field transition: there, $F_{|h|^2}(s) \propto s$ holds for small s (cf. Prop. 4), which results in the more beneficial proportionalities $\epsilon \propto \eta_{\text{opt}}^{-1}$ and $\eta_\epsilon \propto \epsilon$. The improvement stems from polarization diversity.

B. Outage Capacity C_ϵ

We shift our focus to narrowband data communication over this fading channel, with transmit power P_T and reception in additive white Gaussian noise (AWGN) of power P_N . The signal-to-noise ratio $\text{SNR} = |h|^2 P_T / P_N$ is random and the instantaneous channel capacity $C = \log_2(1 + \text{SNR})$, measured in bit/s/Hz, is thus also random and can fade to zero.

A well-established measure for the communication performance of a fading channel is the outage capacity [1, Eq. 5.57]

$$C_\epsilon = \log_2 \left(1 + \frac{F_{|h|^2}^{-1}(\epsilon) \cdot P_T}{P_N} \right) \quad (28)$$

for which, by definition, the event $\log_2(1 + \text{SNR}) < C_\epsilon$ occurs with probability ϵ . We argue that $C_\epsilon \propto F_{|h|^2}^{-1}(\epsilon)$ for small ϵ because the bound $C_\epsilon \leq \log_2(e) \cdot F_{|h|^2}^{-1}(\epsilon) \cdot P_T / P_N$, which is obtained through log-linearization, is tight for low SNR or for a small target ϵ . Hence, by (27), the near- and the far-field regions exhibit the scaling behavior

$$C_\epsilon \propto \epsilon^2. \quad (29)$$

This means that a target outage probability $\epsilon \ll 1$ can only be achieved with an extremely small data rate. In contrary, the near-far-field transition exhibits the more beneficial scaling behavior $C_\epsilon \propto \epsilon$ due to polarization diversity (by Prop. 4).

C. Bit Error Rate p_e

Another popular measure of the communication performance over a fading channel is the bit error rate p_e . For antipodal modulation (BPSK) and reception in AWGN, its value given h is $Q(\sqrt{2\text{SNR}})$ whereby $\text{SNR} = |h|^2 P_T/P_N$ is random and subject to fading. [1, Eq. 3.13]

Proposition 7. Assume (12), AWGN, and either the near-field region ($J_* = J_{\text{NF}}$) or the far-field region ($J_* = J_{\text{FF}}$). Then, the bit error rate of BPSK modulation has the upper bound

$$p_e < \frac{f_{J_*}(0)}{\sqrt{\pi \cdot \text{SNR}_{\text{opt}}}} \quad (30)$$

which becomes tight for large $\text{SNR}_{\text{opt}} = |h_{\text{opt}}|^2 P_T/P_N$.

Proof. $\text{SNR} \approx J_*^2 \text{SNR}_{\text{opt}}$ applies in the near- or far-field region. For the bit error rate we calculate $p_e = \mathbb{E}[Q(\sqrt{2J_*^2 \text{SNR}_{\text{opt}}})] = \int_{-1}^1 f_{J_*}(J_*) Q(\sqrt{2J_*^2 \text{SNR}_{\text{opt}}}) dJ_* \leq 2 \cdot f_{J_*}(0) \int_0^1 Q(\sqrt{2J_*^2 \text{SNR}_{\text{opt}}}) dJ_* = 2 \cdot f_{J_*}(0) \left(\frac{1 - e^{-\text{SNR}_{\text{opt}}}}{\sqrt{4\pi \cdot \text{SNR}_{\text{opt}}}} + Q(\sqrt{2\text{SNR}_{\text{opt}}}) \right)$ and apply $Q(x) < \frac{1}{x} \frac{1}{\sqrt{2\pi}} e^{-x^2/2}$. \square

The large-SNR description in Prop. 7 has the standard form $p_e \propto \text{SNR}_{\text{opt}}^{-L}$ from [1, Eq. 3.158]. We deduce that the diversity exponent is $L = \frac{1}{2}$ for the near- and far-field regions, associated with catastrophic fading (worse than $L = 1$ of Rayleigh fading). In a similar fashion, it can be argued that $p_e \propto \text{SNR}_{\text{opt}}^{-1}$ in the near-far-field transition for large SNR_{opt} , i.e. $L = 1$ (like Rayleigh fading). This is a direct consequence of $f_{|h|}(x) \propto x$ for small x ; the details are omitted.

V. IMPLICATIONS FOR RFID AND BACKSCATTER

So far, the results concerned links with an active TX equipped with a TX amplifier, where $\text{SNR} \approx \text{SNR}_{\text{opt}} J_*^2$ with $J_* \in \{J_{\text{NF}}, J_{\text{FF}}\}$ in the near- or far-field region. For a passive RFID tag that uses load modulation or for backscatter communication, the fading channel applies twice and the relation changes to $\text{SNR} \approx \text{SNR}_{\text{opt}} J_*^4$, cf. [6], with the following severe consequences. The misalignment losses double in terms of dB value (e.g., the abscissa of Fig. 7). Likewise, the bit error rate $p_e \propto \text{SNR}_{\text{opt}}^{-1/4}$ with a diversity exponent of only 1/4.

VI. SUMMARY & CONCLUSIONS

We provided an analytical description of the statistics of the fading channel between two randomly oriented dipoles. Our outage analysis revealed that drastic signal losses are very likely to occur, especially in the near- and far-field regions. This emphasizes the importance of diversity concepts for this class of links, e.g., the use of a rotating source, appropriate antenna polarization, or antenna arrays and beamforming. The results also suggest that, for special applications, it can be favorable to design a link such that the RX will typically be located in the transition region between near and far field.

APPENDIX: PHYSICAL CONDITIONS & DETAILS

The channel coefficient h in (1) relates the power wave emitted by a power-matched TX amplifier to the power wave into a power-matched RX amplifier or tank circuit. A necessary condition for (1) to apply is that h (obtained with this formula) fulfills $|h|^2 \ll 1$, i.e. the dipoles are weakly coupled.

The prefactor $\alpha = \bar{\alpha} e^{-jkr}$ in (1) comprises technical link parameters in $\bar{\alpha}$. For *loop antennas* (i.e. coils), the value $\bar{\alpha} = \frac{j\mu_0 A_T N_T A_R N_R f k^3}{\sqrt{4R_T R_R}}$ applies if the coils are electrically small, the turn pitch angle is small, and the coil diameters are significantly smaller than r . We use the permeability μ_0 , TX- and RX-side number of turns N_T and N_R , the coil areas A_T and A_R , carrier frequency f , wavenumber k , and the TX- and RX-side antenna resistances R_T and R_R . [3, Sec. 5.2]

We note that $\frac{\mu_0}{2\pi} A_T N_T A_R N_R r^{-3} J_{\text{NF}}$ is the mutual inductance M . Furthermore, a small power-matched TX coil is described by a magnetic dipole moment phasor $\mathbf{m} = A_T N_T i_T \mathbf{O}_T$ with current phasor $i_T = \sqrt{P_T/R_T}$ and TX power P_T .

Between *dipole antennas* without ohmic losses, $\bar{\alpha}$ is given by the antenna directivity: $\bar{\alpha} = 1.5$ for electrically small dipole antennas and $\bar{\alpha} \approx 1.64$ for the $\lambda/2$ -length case [3, Cpt. 4].

ACKNOWLEDGEMENT

We would like to thank Robin Kramer for valuable inputs and Bharat Bhatia for helping with the appendix.

REFERENCES

- [1] D. Tse and P. Viswanath, *Fundamentals of Wireless Communication*. Cambridge University Press, 2005.
- [2] E. Biglieri, J. Proakis, and S. Shamai, "Fading channels: Information-theoretic and communications aspects," *IEEE Transactions on Information Theory*, vol. 44, no. 6, pp. 2619–2692, 1998.
- [3] C. A. Balanis, *Antenna Theory: Analysis and Design*. Wiley, 2005.
- [4] D. Cox, "Antenna diversity performance in mitigating the effects of portable radiotelephone orientation and multipath propagation," *IEEE Transactions on Communications*, vol. 31, no. 5, pp. 620–628, 1983.
- [5] C. B. Dietrich, K. Dietze, J. R. Nealy, and W. L. Stutzman, "Spatial, polarization, and pattern diversity for wireless handheld terminals," *IEEE Transactions on Antennas and Propagation*, vol. 49, no. 9, pp. 1271–1281, 2001.
- [6] G. Dumphart and A. Wittneben, "Stochastic misalignment model for magneto-inductive SISO and MIMO links," in *IEEE PIMRC*, Sep. 2016.
- [7] Z. Zhang, E. Liu, X. Qu, R. Wang, H. Ma, and Z. Sun, "Connectivity of magnetic induction-based ad hoc networks," *IEEE Transactions on Wireless Communications*, vol. 16, no. 7, pp. 4181–4191, Jul 2017.
- [8] K. Finkenzeller, *RFID Handbook*. Carl Hanser, 2015.
- [9] C. Angerer, R. Langwieser, and M. Rupp, "RFID reader receivers for physical layer collision recovery," *IEEE Transactions on Communications*, vol. 58, no. 12, pp. 3526–3537, 2010.
- [10] Z. Sun, I. F. Akyildiz, S. Kisseleff, and W. Gerstacker, "Increasing the capacity of magnetic induction communications in RF-challenged environments," *IEEE Transactions on Communications*, vol. 61, no. 9, pp. 3943–3952, 2013.
- [11] M. Soma, D. C. Galbraith, and R. L. White, "Radio-frequency coils in implantable devices: misalignment analysis and design procedure," *IEEE Transactions on Biomedical Engineering*, no. 4, pp. 276–282, 1987.
- [12] K. Fotopoulou and B. W. Flynn, "Wireless power transfer in loosely coupled links: Coil misalignment model," *IEEE Transactions on Magnetics*, vol. 47, no. 2, pp. 416–430, 2011.
- [13] S. J. Orfanidis, *Electromagnetic waves and antennas*. Rutgers University, 2002.
- [14] G. Dumphart, "Magneto-inductive communication and localization: Fundamental limits with arbitrary node arrangements," Ph.D. dissertation, ETH Zürich, 2020.